# DOUBLE-TRACER DOSIMETRY OF ORGANS IN ASSESSMENT OF BONE MARROW INVOLVEMENT BY TWO MONOCLONAL ANTIBODIES

E. Tapani Korppi-Tommola, Kalevi J. A. Kairemo, Antti P. Jekunen, Eero O. Niskanen and Sauli E. Savolainen

Five patients with ductal breast cancer were studied using simultaneous administration of $^{99}Tc^m$-labelled BW250/183 and $^{131}I$-labelled B72.3 monoclonal antibodies (MAbs). The distribution and dosimetry of these tracers were evaluated using the information from simultaneous anterior and posterior whole body scintigrams, together with $^{99}Tc^m$ and $^{131}I$ standard activity sources, recorded on an average of 1, 4, 24, 90 and 224 h after injection. A method to eliminate $^{131}I$ scatter on $^{99}Tc^m$-channel was developed. The geometric means of conjugate views and region-of-interest analysis were used to determine organ uptakes, mean residence times and absorbed radiation dose estimates of organs induced by the tracers. Organ uptakes (% of injected activity/ml) varied from $6.2 \times 10^{-3}$/red marrow to $3.1 \times 10^{-2}$/liver for $^{99}Tc^m$-MAb and from $3.1 \times 10^{-2}$/red marrow to $1.8 \times 10^{-1}$/liver for $^{131}I$-MAb, one hour after injection. Calculated average residence times of organs for $^{99}Tc^m$-labelled BW250/183 were in the range of physical mean-life of $^{99}Tc^m$ and from 71 to 95 h for $^{131}I$-B72.3 respectively. The average total absorbed dose from $^{99}Tc^m$-MAb to the bone marrow was 0.01 and to the spleen 0.14 mGy/MBq and from $^{131}I$-MAb the corresponding values were 0.48 and 10.76 mGy/MBq. This double-tracer technique provides information from two antibodies having different kinetic behaviour and may facilitate in distinguishing various antigens in targeting and control MAb applications.

Monoclonal antibodies (MAbs) have been raised against different types of malignancies for radioimmunoscintigraphy and promising radioimmunotherapy results have been reported (1–3). The dose-limiting organ in radioimmunotheraphy is usually bone marrow (4, 5). In order to protect the critical organs in radioimmunodetection and -therapy procedures there is a need for absorbed organ dose estimation and follow-up.

It was suggested that gamma camera measurement of the activity in the whole skeleton region of interest in

anterior (AP) and posterior (PA) projection provides a way of obtaining both qualitative and semiquantitative evaluation of bone uptake with a single tracer administration in a routine bone scan (6). Dual large-field-of-view gamma camera systems offer faster whole body imaging procedures (7).

To our knowledge, there are no reports of whole body image quantitation using a dual-headed camera in double-tracer studies. In the literature, there are a few clinical reports on single-tracer studies, e.g. determination of thyroid carcinoma metastases and normal residual thyroid absorbed doses from radioiodine-131 using a dual-headed whole body imager with special collimators (8). A special high-resolution collimator system for dual-headed whole body scanner has been designed for imaging and quantifying therapy levels of iodine-131 (9). The distribution and dosimetry of the somatostatin analogue $^{111}In$-DTPA-octreotide in man have been evaluated by using a single dose injection and whole body scintigraphy from two projections (10). Similarly, another group reported the biodistribution and dosimetry for MAb against ovarian carcinoma (11).

The assessment of bone marrow infiltration is important in the evaluation of potential candidates for peripheral blood stem cell transplantation. Routinely, bone scans have been considered as indicators of metastatic growth in the bone marrow. However, bone scintigraphy is not specific for detecting skeletal metastases in breast cancer, as osteoblasts, the targets of bone-seeking tracers in normal bone scans, are increased only in about 50% (12). Using whole body scintigraphy in detecting bone metastases, the $^{99}Tc^m$-labelled MAb scan has been superior (72%) to the conventional bone scan (53%) (3, 4). Therefore, we were interested in investigating bone marrow with radioimmunodetection using double-tracer technique and a double-detector gamma camera. Quantitative scintigraphies were performed for bone marrow-seeking $^{99}Tc^m$-labelled monoclonal antibody BW250/183 recognizing granulocytes and breast cancer derived $^{131}I$-labelled monoclonal antibody B72.3.

The first aim of this study was to establish a precise bone marrow radioimmunoimaging technique, with particular regard to the detection of metastatic lesions of breast cancer using $^{99}Tc^m$-labelled monoclonal antibody BW250/183. Secondly this study was conducted in order to determine whether the simultaneously injected radioimmunotherapy agent, $^{131}I$-labelled monoclonal antibody B72.3, accumulates in the metastases. Thirdly, a dose quantitation method and technique (imaging procedure, scatter correction, region-of-interest analysis) was developed for both tracers involved, based on dual-projection, whole body scintigraphy. Tracer distributions, organ residence times and absorbed doses were calculated.

## Material and Methods

### Monoclonal antibodies

Two intact antibodies of $IgG_1$-subclass were used, BW250/183 (Behringwerke, Marburg, Germany) and B72.3 (Sorin Biomedica, Saluggia, Italy). The former recognizes NCA-95 antigen on granulocytes thus revealing the distribution of normal bone marrow and the latter recognizes TAG-72 antigen on epithelial carcinomas originally extracted from a hepatic metastasis of breast carcinoma. Malignant cells foreign to bone marrow should be visualized as defects with $^{99}Tc^m$-MAb and as uptakes with $^{131}I$-MAb. The amount of BW250/183 injected was 2.00 mg and the amount of B72.3 was 0.50 mg. BW250/183 was labelled directly with $^{99}Tc^m$ by using a reduction technique (Schwartz-method) and B72.3 by Iodogen method.

### Patients

Five breast cancer patients entered the study. Their histories are briefly described below and summarized in Table 1.

*Patient No. 1.* A 59-year-old woman with a ductal breast cancer diagnosed 14 years earlier. At the time of immunoscintigraphy, the disease had spread widely to bone, e.g. vertebrae and ribs. Radiotherapy had been administered to the region of primary operation and palliatively to C-3–Th-1 vertebrae.

*Patient No. 2.* A 68-year-old woman who, 3 years after mastectomy, antioestrogen therapy and chemotherapy, had developed bone metastases in the vertebral columns, ribs, scapulae, right humerus, sacrum, sacro-iliac region, iliac crest and femur. She had received palliative radiotherapy to the right femur and T-11–S1 vertebrae, and lower pelvis.

*Patient No. 3.* A 70-year-old woman with a widely metastasized breast cancer: to the vertebral column, ribs at both sides, proximal humera, right femur and liver. A ductal breast cancer was diagnosed three years earlier, and she had received postoperative radiotherapy to the brain, left femur, right scapula and right femur.

*Patient No. 4.* A 46-year-old woman who had a ductal breast cancer two years earlier and had received postoperative radiotherapy and adjuvant chemotherapy. Despite the treatment, bone scan revealed metastases in both femora, and vertebral column. She had received radiotherapy to the C-4–Th-6 vertebrae and to the right femur and right humerus.

*Patient No. 5.* A 61-year-old woman with a history of succesfully operated lung cancer on the right side in 1988. A ductal breast cancer was diagnosed three years later. She received postoperative radiotherapy. One and a half years later, bone and liver metastases were observed. Despite chemotherapy, the patient developed bone metastases in the ribs, vertebral columns, proximal femora, and left humerus.

### Imaging protocol

Whole body imaging was performed using a Picker 'Prism 2000' dual-detector gamma camera (Picker International Inc., Cleveland, Ohio, USA) equipped with medium energy (300 keV) collimators at approximately 1, 4, 24, 90 and 224 h after simultaneous, slow i.v. injection of 740 MBq $^{99}Tc^m$-BW250/183 and 74 MBq $^{131}I$-B72.3 (5 ml + 5 ml in 0.9% NaCl). In double-tracer imaging the choice of collimator was a compromise between optimal sensitivity and resolution for both isotopes used. In accordance with gamma energies and appropriate imaging properties of $^{99}Tc^m$ and $^{131}I$ isotopes, the best available collimators were used. The thyroid was blocked by using orally administered potassium iodide (400 mg daily) and potassium perchlorate (800 mg daily) for 10 days. Before each imaging, the patient was asked to empty the bladder.

Two separate 20% energy windows were peaked symmetrically at 140 and 364 keV. Radioactive standard sources, about 3.7 MBq/20 ml $^{99}Tc^m$ and 0.7 MBq/10 ml

**Table 1**

*Summary of ductal breast cancer patients*

| Patient/age | Known metastases | Current treatment | Scintigraphy findings |
|---|---|---|---|
| 1/59 | V, R | HT | Tc: +, I: − |
| 2/68 | V, R, E, P | ChT, ERT | Tc: +, I: − |
| 3/70 | V, R, E, S, L | ChT | Tc: +, I: − |
| 4/46 | V, E | ChT | Tc: +, I: − |
| 5/61 | V, R, E, L | ChT | Tc: +, I: − |

Skeletal metastases: V = vertebral columns, R = ribs, E = extremities, P = pelvis, S = skull, Liver metastases = L
Treatment: HT = hormone treatment, ChT = chemotherapy, ERT = external radiation therapy
Scintigraphy: Tc: + = $^{99}$Tc$^m$-BW250/183 true positive, I: − = $^{131}$I-B72.3 false negative

$^{131}$I, were placed 10 cm apart on the imaging pallet between the patient's feet. The activity distributions were recorded simultaneously for $^{99}$Tc$^m$ and $^{131}$I using an automatic body contour follow and scanning speed of 1 mm/s. Each imaging session produced four whole body images, AP and PA images for each tracer. All but one patient, who missed the first two sessions, were imaged five times.

*$^{131}$I scatter correction*

The amount of $^{131}$I scatter in the 140 keV $^{99}$Tc$^m$ window was determined from the last of five $^{131}$I images. Because of the short half-life of $^{99}$Tc$^m$, there was virtually no $^{99}$Tc$^m$ left in the 140 keV window after nine days, only pure Compton scatter of $^{131}$I was available. The scatter correction factor was calculated as a ratio of the information (geometric mean of total counts of the whole AP and PA image matrixes, 256 × 1024 pixels) of the scatter image in the 140 keV window to the information of the original image in the 364 keV window. This ratio was determined individually for each patient. Because the distribution of the tracer in organs was time-dependent, the $^{131}$I scatter image was generated for every $^{99}$Tc$^m$/$^{131}$I image pair by multiplying the series of original$^{131}$I images by the individual scatter correction factor. These $^{131}$I scatter images, with different tracer distributions, were subtracted from the simultaneously recorded original $^{99}$Tc$^m$ images (including $^{131}$I scatter) to produce $^{131}$I scatter free $^{99}$Tc$^m$ images.

*Region-of-interest analysis*

During the analysis 15 different regions-of-interest (ROIs) were applied to 92 whole body images. Activity distributions and outlines of organs were best visualized in the first $^{99}$Tc$^m$ images. ROIs for whole body, different thoracic and abdominal organs, bone marrow and standard sources were drawn on these images and saved, to be

applied to $^{131}$I images and mirrored posterior images. The shape and size of ROIs were kept unchanged throughout the study sequence for each patient. Because of changes in overall patient positioning, ROIs were repositioned independently in each study. The overlapping of organs, right kidney with liver and stomach with spleen, was avoided by drawing ROIs excluding the overlapping organ areas. The possible asymmetry in kidney function was taken into account by using the mean value of kidneys. The ROI for bone marrow was drawn on the proximal end of the femur. The ROI information was presented as number of counts, pixels and average count densities (counts/pixel).

*Organ uptake, mean residence time and absorbed dose calculations*

An assumption for homogeneous tracer distribution and equal attenuation for individual organs and whole body was made. The dose quantitation was based on the use of external standard sources of $^{99}$Tc$^m$ and $^{131}$I with known activity concentrations. The geometric means of all ROI count densities of AP and PA whole body images were calculated. These were related to the decay corrected standard activity concentration. Finally, the calculated data were presented as an organ uptake, percentage of administrated activity/ml, for both tracers, as a function of time. The uptake was calculated in accordance with formulae presented in the appendix.

The time-dependent kinetic behaviour of organ uptakes was assumed to be monoexponential. The logarithm of uptakes as a function of time yielded a linear model. The inverse of the slope fitted with least-squares corresponded to the mean residence time. This was calculated for seven different organs involved, for each patient and separately for both tracers.

Absorbed organ doses and effective doses were determined from both tracers using MIRD formalism (15) and the MIRDOSE 3 program (16), based on calculated mean residence times.

**Results**

No adverse reactions to MAb administration were observed. Table 1. summarizes the patient characteristics and imaging findings. In Fig. 1 there is an example of serial (1, 4, 21, 69 and 237 h after injection) AP whole body images of a patient with vertebral metastases. Fig. 1a illustrates the $^{131}$I scatter-free, whole body distribution of the $^{99}$Tc$^m$-BW250/183 tracer. In the first two images in particular, the body outline, organ sites, bone marrow and the vertebral defects are well visualized. Because of the short half-life of the $^{99}$Tc$^m$-tracer there is hardly anything to be seen in the last two images. As a result of adequate scatter correction, only the $^{99}$Tc$^m$ source of the two external activity standards activity standards is visible. The average amount of
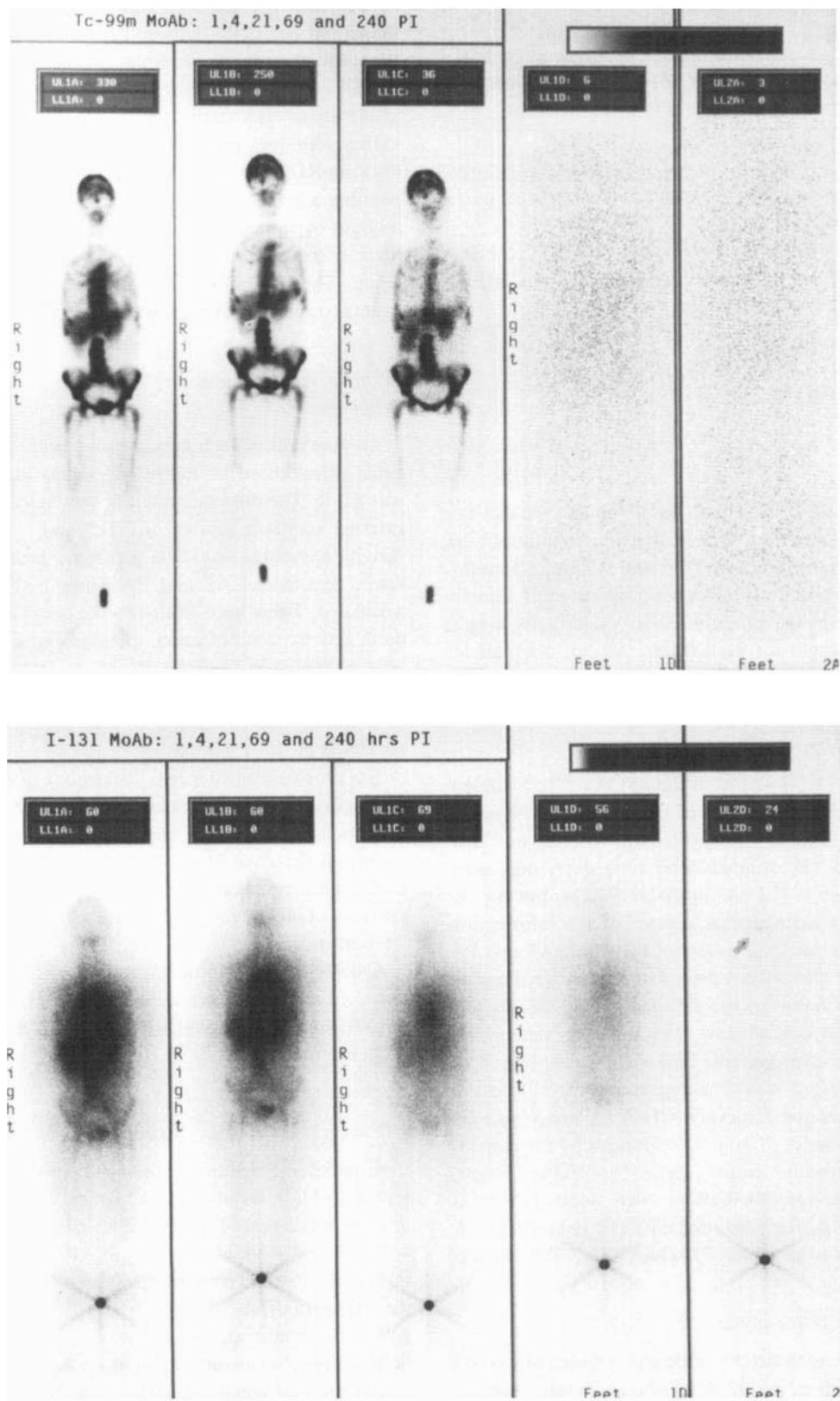
(b)

*Fig. 1.* A typical example of anterior projection whole body scintigrams obtained in consecutive $^{99}Tc^m$-BW250/183 imaging sessions from a patient with metastasized breast carcinoma (Pat. No 1/5). $^{131}I$ scatter subtracted images. An arrow shows a big vertebral lesion a). Corresponding series of $^{131}I$-B72.3 whole body scintigrams of the same patient. Activity remains in circulation. A tiny thyroid uptake is shown and indicated by an arrow, b). However, no specific accumulation in lesion sites was detected with any of the five patients.
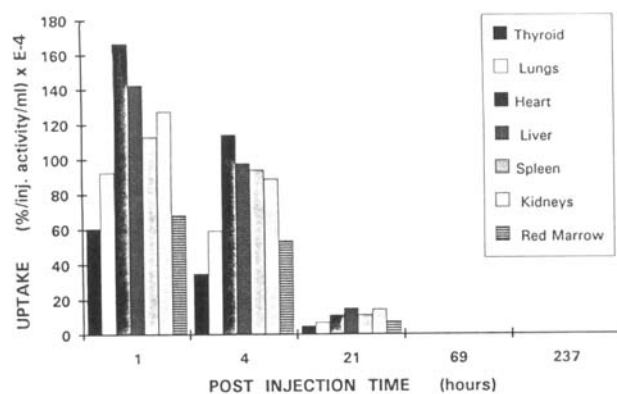
*Fig. 2.* Organ uptake distribution of the MAb tracer $^{99}$Tc$^{m}$-BW250/183 as a function of time. An example of the same patient as in Fig. 1 (Pat. No 1/5). The heart uptake is dominant at 1 and 4 h after injection. Kidneys and liver have highest uptakes at 21 h.

*Fig. 3.* Organ uptake distribution of the MAb tracer $^{131}$I-B72.3 as a function of time, of the same patient (Pat. No 1/5). A longer retention of the tracer is evident. At 69 h the thyroid reaches the spleen uptake and at 237 h the thyroid uptake takes over.

pure $^{131}$I scatter in the 140 keV window, compared with $^{131}$I image information in the 364 keV window, was 45 ± 2%.

A series of simultaneously recorded $^{131}$I-B72.3 whole body images with poor organ visualization is presented in Fig. 1b. The radioactivity remains in the circulation. The increased thyroid uptake was also detected, best seen in the last image. The star-like figure of the external source, clearly seen in the $^{131}$I images, is due to the high activity concentration and the collimator septum penetration of high-energy iodine photons.

Bone marrow lesions with decreased uptake were clearly observed in the $^{99}$Tc$^{m}$-BW250/183 whole body images for all five patients. Some new additional lesions were found compared to earlier bone scans. On the other hand, not a single corresponding lesion with an increased uptake was observed in $^{131}$I-B72.3 whole body images.

Depending on the clinical stage of the cancer patient, the uptake distribution of organs varied from patient to patient. In Fig. 2 there is an example of $^{99}$Tc$^{m}$-BW250/183 uptake distribution of organs as a function of post-injection time. The uptake distribution corresponds to the whole body image presented in Fig. 1. The organ-dependent kinetic behaviour is well demonstrated by this uptake distribution. At one hour the heart uptake is dominant. Kidneys and liver have highest uptakes at 21 h. The uptake of red marrow was approximately half of the kidney uptake. The main trends of the tracer kinetics with the other four patients resembled each other.

The ranges of organ uptakes of the $^{99}$Tc$^{m}$-tracer for all the patients, one hour after injection, were as follows: the bone marrow uptake (percentage of injected activity/ml) varied from $6.3 \times 10^{-3}$ to $1.2 \times 10^{-2}$, heart uptake from $1.6 \times 10^{-2}$ to $2.2 \times 10^{-2}$, liver from $1.4 \times 10^{-2}$ to $3.1 \times 10^{-2}$, kidneys from $9.6 \times 10^{-3}$ to $2.2 \times 10^{-2}$, lungs from $7.4 \times 10^{-3}$ to $1.5 \times 10^{-2}$, spleen from $9.0 \times 10^{-3}$ to $2.0 \times 10^{-2}$ and thyroid from $6.0 \times 10^{-3}$ to $1.1 \times 10^{-2}$.
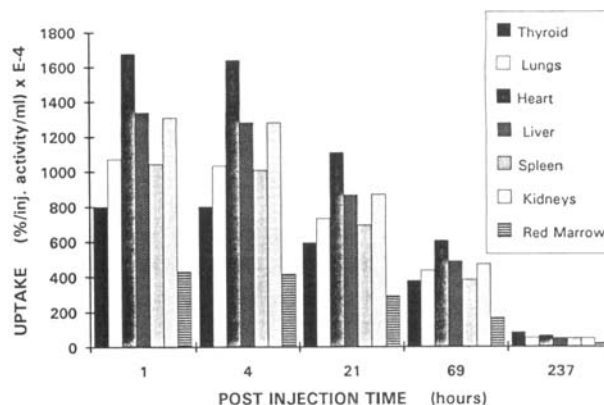
The simultaneous $^{131}$I-B72.3 uptake distribution of the same patient is illustrated in Fig. 3. The biokinetic behaviour $^{131}$I-tracer in different organs is more stable. At one and four hours there is hardly any change in the uptake distribution. At 69 h the thyroid uptake reaches the spleen uptake and at 237 h the thyroid uptake takes over.

The corresponding uptake ranges (at 1 h post injection) for all the patients were from $3.1 \times 10^{-2}$ to $4.7 \times 10^{-2}$ for bone marrow, from $1.2 \times 10^{-1}$ to $1.8 \times 10^{-1}$ for heart, from $1.0 \times 10^{-1}$ to $1.8 \times 10^{-1}$ for liver, from $8.3 \times 10^{-2}$ to $1.3 \times 10^{-1}$ for kidneys, from $7.1 \times 10^{-2}$ to $1.1 \times 10^{-1}$ for lungs, from $8.7 \times 10^{-2}$ to $1.5 \times 10^{-1}$ for spleen and from $5.2 \times 10^{-2}$ to $8.0 \times 10^{-2}$ for thyroid expressed as percentage of injected activity/ml.

Residence times of organs for $^{99}$Tc$^{m}$-BW250/183 are listed in Table 2. To determine the slowest component of

**Table 2**

$^{99}$Tc$^{m}$-MAb mean residence times (hours)

| Patient | Thyroid | Lungs | Heart | Liver | Spleen | Kidneys | R Marr |
|---|---|---|---|---|---|---|---|
| All 5 studies | | | | | | | |
| 1 | 9.2 | 9.1 | 8.9 | 8.9 | 9.0 | 8.9 | 9.0 |
| 3 | 10.9 | 10.9 | 10.5 | 10.4 | 10.8 | 10.6 | 11.0 |
| 4 | 9.2 | 9.1 | 9.0 | 8.9 | 9.1 | 9.1 | 9.2 |
| 5 | 8.8 | 8.8 | 8.7 | 8.5 | 8.7 | 8.7 | 8.9 |
| Average | 9.5 | 9.5 | 9.3 | 9.2 | 9.4 | 9.4 | 9.5 |
| Three latest studies | | | | | | | |
| 1 | 9.0 | 9.0 | 8.9 | 8.7 | 8.8 | 8.8 | 8.8 |
| 2* | 9.4 | 9.4 | 9.2 | 9.1 | 9.0 | 9.3 | 9.2 |
| 3 | 10.7 | 10.8 | 10.5 | 10.1 | 10.6 | 10.3 | 10.9 |
| 4 | 9.3 | 9.3 | 9.3 | 9.1 | 9.4 | 9.5 | 9.4 |
| 5 | 9.1 | 9.3 | 9.3 | 8.8 | 9.2 | 9.3 | 9.3 |
| Average | 9.5 | 9.5 | 9.4 | 9.2 | 9.4 | 9.4 | 9.5 |

* Only late studies done.

## Table 3

$^{131}I$-MAb mean residence times (hours)

| Patient | Thyroid | Lungs | Heart | Liver | Spleen | Kidneys | R Marr |
|---|---|---|---|---|---|---|---|
| All 5 studies | | | | | | | |
| 1 | 105.8 | 79.6 | 73.5 | 73.5 | 79.3 | 73.3 | 81.9 |
| 3 | 90.4 | 74.4 | 65.9 | 65.5 | 71.9 | 71.0 | 86.9 |
| 4 | 75.9 | 72.8 | 72.0 | 69.2 | 71.2 | 69.3 | 76.2 |
| 5 | 82.1 | 80.6 | 78.0 | 77.5 | 79.6 | 80.2 | 84.1 |
| Average | 88.6 | 76.8 | 72.3 | 71.4 | 75.5 | 73.5 | 82.3 |
| Three latest studies | | | | | | | |
| 1 | 111.1 | 81.7 | 76.2 | 76.1 | 82.9 | 75.9 | 85.2 |
| 2* | 104.6 | 102.8 | 99.0 | 102.7 | 107.6 | 114.0 | 125.1 |
| 3 | 91.4 | 75.5 | 66.5 | 66.1 | 72.0 | 70.4 | 87.9 |
| 4 | 82.1 | 80.6 | 78.0 | 77.5 | 79.6 | 80.2 | 84.1 |
| 5 | 84.5 | 74.2 | 70.2 | 71.9 | 73.9 | 77.0 | 86.5 |
| Average | 94.7 | 83.0 | 78.0 | 78.9 | 83.2 | 83.5 | 93.7 |

* Only late studies done.

the tracer kinetics and to evaluate the validity of the monoexponential model, the results are presented in two ways: first, including all 5 studies; and secondly, including only 3 of the latest studies, from 24 to 224 h post injection. In particular, with a slower disappearing tracer $^{131}I$-B72.3, the one compartment model fits less well and the importance of the 3 latest studies becomes more apparent, as increased residence times, as seen in Table 3. In dose evaluation the slowest component causes the highest dose.

Radiation doses absorbed by different organs are listed in Tables 4 and 5. In addition, effective doses are presented. The average effective dose for the $^{99}Tc^{m}$-BW250/

183 tracer was 0.05 mSv/MBq and for the $^{131}I$-B72.3 tracer 4.1 mSv/MBq.

### Discussion

The basic purpose of this study was to use one tracer for exact imaging of bone marrow and the other as a candidate for radioimmunotherapy, for the imaging of metastases. Both tracers were needed for the quantization of absorbed dose. In particular, the organ dose calculation for the $^{131}I$-tracer could not be made without the additional anatomical information produced by the $^{99}Tc^{m}$-tracer. The dual-detection eliminated the depth dependency of organ absorption.

In our approach, non-invasive estimations of the absorbed organ and red marrow doses were based on scintigraphic information. The clear visualization of the body outline and the different organs was mandatory. The $^{99}Tc^{m}$-labelled tracer had excellent imaging properties which resulted in accurate visualization of organs, bone marrow, and metastatic sites, which appeared as cold spots. On the other hand the visualization of organs on $^{131}IMAb$-scans is diffuse and limited for organ delineation. As referred to earlier, there have been trials to improve the resolution of $^{131}I$-MAb-scans by using specially planned high-energy and high-resolution collimation systems, not commercially available for normal gamma cameras. However, the delineation of organs can readily be performed by using the double-tracer technique described in this study.

Several authors have reported that bone marrow scintigraphy is more sensitive than bone marrow scanning in detecting bone metastases from prostate and breast cancer

## Table 4

$^{99}Tc^{m}$-MAb absorbed radiation doses (mGy/MBq)

| Patient | Thyroid | Lungs | Heart | Liver | Spleen | Kidneys | R Marr | Eff Dose |
|---|---|---|---|---|---|---|---|---|
| All 5 studies | | | | | | | | ** |
| 1 | 0.515 | 0.027 | 0.051 | 0.030 | 0.138 | 0.087 | 0.009 | 0.036 |
| 3 | 0.632 | 0.030 | 0.070 | 0.039 | 0.144 | 0.085 | 0.011 | 0.045 |
| 4 | 0.645 | 0.029 | 0.042 | 0.031 | 0.128 | 0.081 | 0.011 | 0.045 |
| 5 | 0.501 | 0.024 | 0.041 | 0.035 | 0.143 | 0.086 | 0.008 | 0.036 |
| Average | 0.573 | 0.027 | 0.051 | 0.034 | 0.138 | 0.085 | 0.010 | 0.041 |
| Three latest studies | | | | | | | | ** |
| 1 | 0.419 | 0.022 | 0.039 | 0.033 | 0.149 | 0.104 | 0.010 | 0.032 |
| 2* | 0.556 | 0.022 | 0.038 | 0.032 | 0.207 | 0.070 | 0.012 | 0.040 |
| 3 | 0.597 | 0.021 | 0.043 | 0.048 | 0.133 | 0.121 | 0.012 | 0.043 |
| 4 | 0.899 | 0.031 | 0.038 | 0.040 | 0.114 | 0.061 | 0.010 | 0.058 |
| 5 | 0.939 | 0.022 | 0.029 | 0.050 | 0.109 | 0.057 | 0.009 | 0.060 |
| Average | 0.682 | 0.024 | 0.038 | 0.041 | 0.142 | 0.083 | 0.010 | 0.050 |

* Only late studies done, ** units in mSv/mBq.

## Table 5

$^{131}I$-MAb absorbed radiation doses (mGy/MBq)

| Patient | Thyroid | Lungs | Heart | Liver | Spleen | Kidneys | R Marr | Eff Dose |
|---------|---------|-------|-------|-------|--------|---------|--------|----------|
| All 5 studies | | | | | | | | ** |
| 1 | 76.00 | 1.87 | 2.85 | 1.44 | 9.24 | 5.86 | 0.37 | 4.54 |
| 3 | 58.20 | 1.64 | 2.59 | 1.37 | 9.73 | 5.04 | 0.38 | 3.56 |
| 4 | 54.10 | 1.72 | 2.51 | 1.39 | 9.23 | 5.09 | 0.42 | 3.36 |
| 5 | 48.60 | 1.62 | 2.59 | 1.54 | 10.20 | 5.33 | 0.35 | 3.06 |
| Average | 59.23 | 1.71 | 2.64 | 1.44 | 9.60 | 5.33 | 0.38 | 3.63 |
| Three latest studies | | | | | | | | ** |
| 1 | 87.60 | 1.95 | 2.91 | 1.44 | 9.58 | 6.00 | 0.39 | 5.18 |
| 2* | 82.90 | 2.48 | 3.78 | 1.89 | 14.80 | 7.04 | 0.65 | 5.11 |
| 3 | 63.00 | 1.60 | 2.49 | 1.36 | 9.39 | 5.22 | 0.45 | 3.82 |
| 4 | 63.70 | 1.90 | 2.87 | 1.46 | 10.20 | 5.24 | 0.50 | 3.92 |
| 5 | 56.80 | 1.79 | 2.72 | 1.46 | 9.82 | 5.10 | 0.41 | 3.52 |
| Average | 70.80 | 1.94 | 2.95 | 1.52 | 10.76 | 5.72 | 0.48 | 4.09 |

* Only late studies done, ** units in mSv/MBq.

(17, 18). It has also been concluded that bone marrow scintigraphy provides complementary information to distinguish benign from malignant lesions (19). However, bone marrow defects may have a variety of causes, e.g. inflammatory, circulatory or degenerative changes, fibrosis, fatty degeneration, necrosis, extensive osteoarthritis, and fatty or bone islands (20–23).

Focal tumour involvement of the bone marrow may result in a random marrow biopsy failing to detect the lesion. Marrow scan is also helpful when examining the extent of active bone marrow in previously treated patients. While chemotherapy causes generalized depression of uptake, radiotherapy results in depressed uptake within the irradiated fields. The techniques described in this article can be used to determine whether sufficient activity can be accumulated in tumours to provide a therapeutic effect, while minimizing irradiation of normal tissue by avoiding administrations which do not provide sufficient radiation dose to the tumour.

In this study it has been shown that in addition to immunoscintigraphy and -therapy the double-tracer technique can be used for estimation of organ dose calculation. In successful radioimmunotherapy it may also be used as a tumor dose follow-up tool. It is worth emphasizing that the imaging procedure is not routine and has to be performed carefully. The delineation of organs for dosimetric calculations is much more accurate on $^{99}Tc^m$ scans; therefore simultaneous acquisition implies that uptake values of various organs, calculated for iodine, are also reliable. Thereby $^{131}I$ scatter has to be taken into consideration and properly subtracted from $^{99}Tc^m$ images.

The results in Tables 2, 3, 4 and 5 were presented separately for all studies and for late studies. There were

two reasons for this presentation. First, one patient missed the first two studies and, secondly, there was a need to test the validity of the one compartment model. This is shown as the difference in the average values of residence times and absorbed doses. The smaller the difference, the better the model. Because of the long half-life of intact MAb (3) and the short half-life of $^{99}Tc^m$, the effective half-life of $^{99}Tc^m$-tracer comes close to the physical half-life of $^{99}Tc^m$. The model fits, as the results in Tables 2 and 4 show. For $^{131}I$-tracer there is a clear difference, $11 \pm 5\%$ increase in average absorbed dose values. This means that the latest studies with the slowest tracer residence components have to be emphasized when using a single-compartment model for dose calculations or another compartment has to be added to the model.

Average mean residence times, listed in Table 2, are systematically (about 7%) higher than the physical mean-life of $^{99}Tc^m$ (8.67 h). This is due to several factors affecting measured and calculated image information. The compromised collimation of double-isotope studies yields to a suboptimal scatter correction. In our case, when using medium energy collimator, high-energy ( > 300 keV) photons of $^{131}I$ cause septal penetration artefacts, as can be seen in Fig. 1b. These additional scatter counts are present in the MAb distribution also and are included in the ROI count densities of different organs. However, these scatter counts are not included in the small standard source ROI. This is why the additional counts from the septal penetration result in an overestimation of organ uptakes and explains the systematic error in mean residence times of the $^{99}Tc^m$-tracer. More additional scatter counts will be present as a result of the scatter of $^{99}Tc^m$ itself. On the other hand, the poor count statistics of $^{99}Tc^m$ in later

studies and the $^{131}$I-scatter image subtraction can cause underestimation of the ROI count densities.

The average bone marrow dose (0.01 mGy/MBq) from the $^{99}$Tc$^m$-tracer calculated in this study is equal to the results disclosed by Duncker et al. (13). The average effective dose (0.05 MSv/MBq) of $^{99}$Tc$^m$-BW 250/183 was negligible compared with that (4.09 mSv/MBq) of $^{131}$I-B72.3. The absorbed dose values of whole body for $^{131}$I-B72.3 are of the same order as those presented by Meredith et al. (24). The $^{99}$Tc$^m$-antibody uptake and lesion detection was high, but the persistent blood pool in the early hours complicated image interpretation, particularly with $^{131}$I antibody images. Thus the kinetic behaviour of different tracers has to be known in order to disclose an optimal therapeutic effect and imaging time. The kinetic behaviour of optimal tracers should be in balance with the physical half-lives of the isotopes used. In this sense, neither of the tracers used in this study was optimal.

The image quality of the $^{99}$Tc$^m$ labelled BW250/183 antibody scan was superior to a bone scan. In the evaluation of bone marrow we found all lesions that were revealed by bone scan, as well as some new defects not detected in earlier bone scans, but we failed to detect any metastatic lesion in $^{131}$I-B72.3 immunoscintigraphy, as our criterion for a metastasis was a clearly defined focus of increased antibody uptake in haematopoietic bone marrow. However, this double-tracer technique yields information from two antibodies having totally different kinetic behaviour and can be applied to any control and targeting MAb applications, preferably with $^{123}$I or some other new promising labels.

## REFERENCES

1. Rosen ST, Zimmer AM, Goldman-Leikin R, et al. Radioimmunodetection and radioimmunotherapy of cutaneous T cell lymphomas using an $^{131}$I-labeled monoclonal antibody: an Illinois Cancer Council study. J Clin Oncol 1987; 5: 562–73.
2. Stewart JSW, Hird V, Snook D, et al. Intraperitoneal $^{90}$Y-labelled monoclonal antibody in ovarian cancer. J Clin Oncol 1990; 8: 1941-50.
3. Kairemo KJA, Liewendahl K. Radioimmunodetection of malignant solid tumours. Scand J Clin Lab Invest 1994; 54: 569–83.
4. Plaizier MABD, Roos JC, Teule GJJ, et al. Comparison of non-invasive approaches to red marrow dosimetry for radiolabelled monoclonal antibodies. Eur J Nucl Med 1994; 21: 216-22.
5. Eary JF, Press OW, Badger CC, et al. Imaging and treatment of B-cell lymphoma. J Nucl Med 1990; 31: 1257-68.
6. D'Addabbo A, Rubini G, Mele M, Lauriero F. A new method for assessing $^{99}$Tc$^m$-MDP bone uptake from a bone scan image: quantitative measurement of radioactivity in global skeletal regions of interest. Nucl Med Commun 1992; 13: 55–60.
7. MacIntyre WJ, Saha GB, Go RT. Planar imaging with single-head large-field-of-view cameras: are they still the workhorse? Semin Nucl Med 1994; 24: 11-6.
8. O'Connell MEA, Flower MA, Hinton PJ, Harmer CL, McCready VR. Radiation dose assessment in radioiodine therapy.

9. Flower MA, Schlesinger T, Hinton PJ, et al. Radiation dose assessment in radioiodine therapy. 2. Practical implementation using quantitative scanning and PET, with initial results on thyroid carcinoma. Radiother Oncol 1989; 15: 345-57.
10. Bajc M, Palmer J, Ohlsson T, Edenbrandt L. Distribution and dosimetry of $^{111}$In DTPA-D-Phe-octreotide in man assessed by whole body scintigraphy. Acta Radiol 1994; 35: 53–7.
11. Buijs WCAM, Massuger LFAG, Claessens RAMJ, Kenemans P, Corstens FHM. Dosimetric evaluation of immunoscintigraphy using indium-111-labeled monoclonal antibody fragments in patients with ovarian cancer. J Nucl Med 1992; 33: 1113–20.
12. Taube T, Elomaa I, Blomqvist C, Beneton MNC, Kanis JA. Histomorphometric evidence for osteoclast-mediated bone resorption in metastatic breast cancer. Bone 1994; 15: 161-6.
13. Duncker CM, Carrió I, Berná L, et al. Radioimmune imaging of bone marrow in patients with suspected bone metastases from primary breast cancer. J Nucl Med 1990; 31: 1450-5.
14. Rieker O, Grünwald F, Layer G, et al. Disseminated bone marrow metastases from primary breast cancer: Detection and follow-up by radioimmune bone marrow scintigraphy. J Nucl Med 1994; 35: 1485-7.
15. Snyder WS, Fisher Jr HL, Ford MR, Warner GG. Estimates of absorbed fractions for monoenergetic photon sources uniformly distributed in various organs of a heterogeneous phantom. MIRD Pamphlet no 5, J Nucl Med 1969; 10 (Suppl 3): 7–52.
16. MIRDOSE 3. Radiation Internal Dose Information Center, Oak Ridge Institute for Science and Education. P.O. Box 117, Oak Ridge, TN 37831, USA.
17. Haddock G, Gray HW, McKillop JH, Bessent RG. $^{99}$Tc$^m$-nanocolloid bone marrow scintigraphy in prostatic cancer. Br J Urol 1989; 63: 497–502.
18. Bourgeois P, Gassavelis C, Malarme M, Feremans W, Frühling J. Bone marrow scintigraphy in breast cancer. Nucl Med Commun 1989; 10: 389-400.
19. Sacchi S, Marietta M, Rinaldi D, et al. Bone and bone marrow scintigraphy in the diagnosis of metasplastic involvement of the skeletal system. J Nucl Med All Sci 1987; 31: 255-60.
20. Vogler III JB, Murphy WA. Bone marrow imaging. Radiology 1988; 168: 679-93.
21. Reske SN, Karstens JH, Gloeckner W, et al. Radioimmunoimaging for diagnosis of bone marrow involvement in breast cancer and malignant lymphoma. Lancet 1989; 1: 299–301.
22. Carpani de Kaski M, Peters AM, Knight D, Stuttle AWJ, Lavender JP, Hodgson HJ. Indium-111 whole-body retention: a method for quantification of disease activity in inflammatory bowel disease. J Nucl Med 1992; 33: 756-62.
23. Peters AM. The utility of [99mTc]HMPAO-leukocytes for imaging infection. Semin Nucl Med 1994; 24: 110-27.
24. Meredith RF, Khazaeli MB, Plott WE, et al. Phase I trial of iodine-131-chimeric B72.3 (human IgG4) in metastatic colorectal cancer. J Nucl Med 1992; 33: 23-9.

## APPENDIX

Organ uptake, $U_{ORG}$, for $^{99}$Tc$^m$-tracer was calculated according to the following formulae.

$$U_{ORG} (^{99}Tc^m) = C_{st\ dc} * (R_{ORG/st}/A_{ADM}) * 100$$

in percentage of injected activity per ml, where

$$C_{st\ dc} = (A_{st}/V_{st}) \bullet \exp(-k_{tc} * t_{acc})$$

the decay corrected concentration of $^{99}Tc^m$ standard source, where

$A_{st}$ = activity of $^{99}Tc^m$ standard source in MBq
$V_{st}$ = volume of $^{99}Tc^m$ standard source in ml
$k_{tc}$ = decay constant of $^{99}Tc^m$ isotope
$t_{acc}$ = post injection time

$$R_{ORG/st} = \sqrt{(OCd_{AP} * OCd_{PA})}/\sqrt{(SCd_{AP} * SCd_{PA})}$$

the ratio of organ counts to standard source counts, with depth correction by geometric mean, where

$OCd_{AP}$ = organ count density in AP image
$OCd_{PA}$ = organ count density in PA image
$SCd_{AP}$ = standard source count density in AP image
$SCd_{PA}$ = standard source count density in PA image
$A_{ADM}$ = the injected $^{99}Tc^m$ activity in MBq

Calculations for $^{131}I$-tracer were made accordingly and for every organ separately.